THE 25TH CHESAPEAKE SAILING YACHT SYMPOSIUM
ANNAPOLIS, MARYLAND, MARCH 2025

A Comparative Study of Control Algorithms on Wind-Powered Cargo Vessel Performance

Martin Kjellberg
Research Institutes of Sweden AB, Sweden, martin.kjellberg@ri.se

Luis Felipe Sánchez-Heres
Research Institutes of Sweden AB, Sweden

Frederik Gerhardt
Research Institutes of Sweden AB, Sweden

Sofia Werner
Research Institutes of Sweden AB, Sweden

Abstract. Wind propulsion for commercial cargo ships is rapidly emerging as a viable technology to reduce greenhouse gas emissions. Naval architects frequently adapt methods and tools originally designed for sailing yachts to create these modern "sailing" vessels. Typically, steady-state Performance Prediction Programs (PPPs) are used to estimate vessel speed, leeway, heel, and other factors under various wind conditions. However, these tools do not account for dynamic factors such as unsteady sail forces due to ship motions in waves, gusty winds, or the vessel's control system dynamics. This paper presents a comparative analysis of control algorithms and their impact on the performance of a wind-powered cargo vessel. We utilize a Dynamic Performance Prediction Program (DPPP) that integrates an unsteady 3D fully nonlinear potential flow hydrodynamic solver with an efficient lifting-line aerodynamic model. This approach allows us to assess the performance implications of different control strategies. The findings reveal how various control strategies influence sailing performance, highlighting the potential benefits and trade-offs in unsteady, real-world environmental conditions.

Keywords: wind propulsion; wind-powered ships; DPPP, sheeting, control algorithms, wing sails

NOMENCLATURE

f	Sheet angle mapping function to apparent wind angle.
t	Time coordinate [s].
$\overline{u}_{\mathrm{air}}$	Mean wind speed [m s^{-1}].
u_{air}	Total longitudinal wind velocity [m s^{-1}].
u_{turb}	Longitudinal turbulence velocity component [m s^{-1}]
v_{turb}	Transverse turbulence velocity component [m s^{-1}].
w_{turb}	Vertical turbulence velocity component [m s^{-1}].
$F_{\mathrm{x,sails}}$	Longitudinal sail force [N].
$F_{\mathrm{x,prop}}$	Longitudinal propeller force [N].

Downloaded from http://onepetro.org/SNAMECSYS/proceedings-pdf/CSYS25/CSYS25/D021S005R003/4625024/sname-csys-2025-015.pdf/1 by Martin Kjellberg on 28 May 2025

H_S Significant wave height [m].
K_P Coefficient for the proportional PID term [-].
P_D Delivered power [W].
T Time constant [s].
T_I Coefficient for the proportional PID term [-].
T_Z Zero up-crossing period [-].
U_{10} Reference wind speed at an elevation of 10 m above the calm water surface [m s^{-1}].

$\boldsymbol{V}_{AW}$ Apparent wind velocity vector [m s^{-1}].
$\boldsymbol{V}_{TW}$ True wind velocity vector [m s^{-1}].
$\boldsymbol{V}_S$ Horizontal velocity vector of the ship [m s^{-1}].
$\boldsymbol{X}$ Position vector in the Earth-fixed frame of reference [m].

Θ Mean wind velocity direction [°]
ψ Heading angle [°]

ABL Atmospheric boundary layer
AWA Apparent wind angle
COG Course over ground
DPPP Dynamic performance prediction program
LIDAR Light detection and ranging
PIC Predictive intermittent control
PID Proportional–integral–derivative (controller)
PPP Performance prediction program
PR Propulsive ratio
PSD Power spectral density
RCC Reactive continuous control
RIC Reactive intermittent control
SA Sheet angle
TWA True wind angle
UAV Unmanned aerial vehicle
VPP Velocity prediction program
6DOF 6 degrees of freedom

1. INTRODUCTION

The sailing performance of a ship equipped with a wind propulsion system (WPS) is significantly influenced by the control of its sails and rudder. The choice of control strategies and algorithms becomes increasingly critical in larger waves and gustier wind conditions. Effective sheet control, which relies on accurate wind sensing, is essential for optimizing performance. However, there is limited literature on this topic.

This paper focuses on sheet control, assuming ideal wind sensing and forecasting capabilities, to explore the potential of various control strategies. We propose three distinct sheet control algorithms and examine their impact on the sailing performance of a general cargo vessel. These algorithms are designed to be simple and straightforward to implement, providing a foundation for future enhancements and increased complexity. Through this study, we aim to assess the performance implications of different control strategies.

Future research will involve the development of models for remote wind field sensing, such as using LIDAR technology, and forecasting the wind conditions that the vessel will encounter in the near future. This will potentially enable more precise and adaptive control strategies compared to current local on-board sensing, further enhancing the performance of wind propulsion systems.

Downloaded from http://onepetro.org/SNAMECSYS/proceedings-pdf/CSYS25/CSYS25/D021S005R003/4625024/sname-csys-2025-015.pdf/1 by Martin Kjellberg on 28 May 2025

2. THEORY

The existing DPPP used in this study, the commercial panel code SHIPFLOW MOTIONS, integrates a 6DOF seakeeping and manoeuvring model for hydrodynamic and aerodynamic hull forces with an efficient lifting-line aerodynamic model for wing sail forces and a spatio-temporal wind model for gusty and turbulent ambient wind, as illustrated schematically in Figure 1. The focus of this paper and the novel contribution is, however, the control algorithms for the wing sails.

Figure 1 Overview of the main building blocks of the DPPP, including the wing sail control algorithms.

The first three blocks are described briefly in the following subsections and more information can be found in (Kjellberg et al., 2023). A more in-depth description of the wing sail control algorithms is given in section 3.

2.1 Seakeeping and Manoeuvring Model

The commercial panel code SHIPFLOW MOTIONS serves as a solver for hydrodynamics and 6DOF rigid body motions. This unsteady 3D fully nonlinear potential flow hydrodynamic model is enhanced with viscous manoeuvring derivatives and appendage forces. Additionally, it incorporates a representation of a short-crested irregular incident wave field (Kjellberg et al., 2023).

2.2 Lifting Line Wing-Sail Model

The wing sail forces are modeled using the quasi-3D sectional integration with lifting-line (CORR-SILL) method described by Malmek et al. (2020). This method combines viscous sectional 2D lift and drag coefficients with lifting-line theory to account for 3D effects, including stall and viscous drag, compare for example Anderson et al. (1980). Aerodynamic interactions between wing sails are managed by iteratively updating and considering the induced velocity from bound and free wake vortices of each wing sail. Currently, no hull-wing interaction is considered. The wing sail model considers the 6DOF motions and velocities of the vessel.

2.3 Spatio-Temporal Wind Model

The spatio-temporal over-water wind model is based on the model proposed by Cole (2018), where it was used for studying the effects of wind on the stability, manoeuvrability and formation control laws for unmanned aerial vehicles (UAV) in an over-water environment, but extended from two spatial dimensions, i.e. horizontally, to three, where also the vertical dimension is considered (Kjellberg et al., 2023).

Downloaded from http://onepetro.org/SNAMECSYS/proceedings-pdf/CSYS25/CSYS25/D021S005R003/4625024/sname-csys-2025-015.pdf/1 by Martin Kjellberg on 28 May 2025

To illustrate, the 3D turbulence velocity component power spectral density (PSD) functions for a mean wind speed $\bar{u}_{\mathrm{air}}$ of 7 m/s at an elevation of 18.6 m above sea level are plotted in Figure 2 together with the mean atmospheric boundary layer (ABL) profile and time series realizations of the individual turbulence velocity components $u_{\mathrm{turb}}(z,t)$, $v_{\mathrm{turb}}(z,t)$, $w_{\mathrm{turb}}(z,t)$ and the total longitudinal velocity $u_{\mathrm{air}}(z=18.6,t)$, i.e. the sum of the mean wind speed $\bar{u}_{\mathrm{air}}(z=18.6)$ and the longitudinal turbulence component $u_{\mathrm{turb}}(z,t)$.

Considering a mean wind velocity direction of Θ, the total wind velocity vector, i.e. true wind velocity, at time t and position (x,y,z) is obtained by adding the turbulence velocity to the mean wind speed power-law profile due to the atmospheric boundary layer:

$$\boldsymbol{V}_{TW}(x,y,z,t)=\begin{bmatrix}\left(u_{\mathrm{turb}}(x,y,z,t)+\bar{u}_{\mathrm{air}}(z)\right)\cos(\Theta)+v_{\mathrm{turb}}(x,y,z,t)\sin(\Theta)\\ \left(u_{\mathrm{turb}}(x,y,z,t)+\bar{u}_{\mathrm{air}}(z)\right)\sin(\Theta)+v_{\mathrm{turb}}(x,y,z,t)\cos(\Theta)\\ w_{\mathrm{turb}}(x,y,z,t)\end{bmatrix} \quad (1)$$

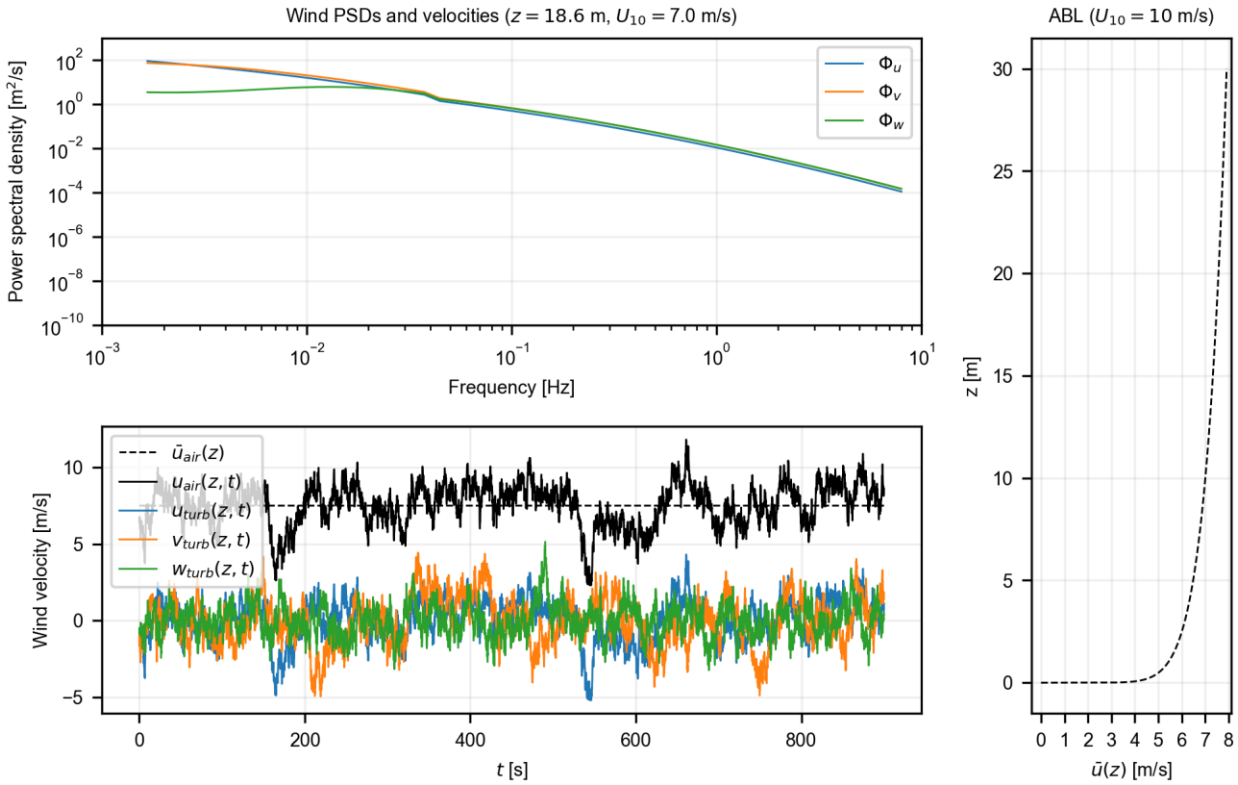

Figure 2. Top: 3D turbulence velocity component PSD functions for a mean wind speed of 7 m/s at an elevation of 18.6 m above sea level. Bottom: A corresponding 900 s time realization of the total and mean (longitudinal) wind speed and the three linear turbulence velocity components. Right: Mean wind speed power-law profile due to the atmospheric boundary layer (ABL) with an exponent of 1/9.

3. CONTROL ALGORITHMS

3.1 Wing Sails

Three different control algorithms for the wing sails are implemented:

1. Reactive Continuous Control (RCC)
2. Reactive Intermittent Control (RIC)
3. Predictive Intermittent Control (PIC)

Downloaded from http://onepetro.org/SNAMECSYS/proceedings-pdf/CSYS25/CSYS25/D021S005R003/4625024/sname-csys-2025-015.pdf/1 by Martin Kjellberg on 28 May 2025

The first two, RCC and RIC, are *reactive* in the sense that they consider past or current wind conditions. They also only rely on local on-board wind measurements. The third, PIC, is called *predictive* as it considers also predicted future wind conditions. In practice, the predictive approach would have to rely on remote sensing of the upstream wind field, e.g. by means of LIDAR, and forecasting the wind conditions that the vessel will encounter some time into the future.

While the RCC continuously adjusts the sheet angles, the RIC and PIC make intermittent adjustments based on when the apparent wind angle has changed more than a given threshold value. Continuous sheeting should perform better from a purely aerodynamic point-of-view, but it is likely to cause more wear on the mechanical systems and use more energy compared to intermittent sheeting and the latter may therefore be an attractive and perhaps more realistic approach.

In this paper, the fact that the spatio-temporal wind model is deterministic means that we can easily sample the wind exactly at any point in time and space and the only thing that must be predicted is the future position of the vessel in space, its velocity and its heading, which is relatively easy to do. This represents close to ideal forecasting capabilities and the result from using the PIC shows the near maximum potential of the approach in terms of the remote sensing and forecasting capabilities.

All three algorithms make use of a pre-determined mapping function f of apparent wind angle AWA to sheet angle SA of each individual sail that maximizes the total longitudinal component, i.e. driving force, of the whole rig:

$$\mathrm{SA} = f(\mathrm{AWA}). \tag{2}$$

In this work, the mapping was done with the vessel in upright condition, assuming small heel angles, although it could be made to include heel angle as an additional parameter to AWA.

The difference between the three approaches lies in the calculation of the apparent wind angle. In general, the apparent wind velocity at time t and at the position $\boldsymbol{X}(t)$ is defined as:

$$\boldsymbol{V}_{AW}(\boldsymbol{X}(t), t) = \boldsymbol{V}_{TW}(\boldsymbol{X}(t), t) - \boldsymbol{V}_{\mathrm{S}}(t) = \begin{bmatrix} u_{AW}(\boldsymbol{X}(t), t) \\ v_{AW}(\boldsymbol{X}(t), t) \\ w_{AW}(\boldsymbol{X}(t), t) \end{bmatrix}, \tag{3}$$

where

$$\boldsymbol{V}_{\mathrm{S}}(t) = \big(v_x(t), v_y(t), 0\big) \tag{4}$$

is the ship's horizontal velocity. The apparent wind angle relative to the heading can then be calculates as:

$$\mathrm{AWA}\big(\boldsymbol{V}_{AW}(\boldsymbol{X}(t), t), \psi(t)\big) = \mathrm{AWA}\big(\boldsymbol{V}_{TW}(\boldsymbol{X}(t), t), \boldsymbol{V}_{\mathrm{S}}(t), \psi(t)\big) = \operatorname{atan2}\left(\frac{v_{AW}(\boldsymbol{X}(t), t)}{u_{AW}(\boldsymbol{X}(t), t)}\right) - \psi(t). \tag{5}$$

More specifically, the position $\boldsymbol{X}(t) = (x(t), y(t), z)$ is here chosen as the geometrical centroid of the rig and z is the vertical position of the centroid at rest. Note that this choice of position is somewhat arbitrary, and another potential choice could, for example, have been at, or slightly above the wing tips where anemometers can be fitted. This is also the vertical position that was used when mapping the sheet angles to apparent wind angle.

The following subsections detail the different algorithms further.

3.1.1 Reactive Continuous Control

RCC operates as a feedback control system where the sheet angle $\mathrm{SA}(t)$ is continuously updated based on the instantaneous apparent wind angle:

Downloaded from http://onepetro.org/SNAMECSYS/proceedings-pdf/CSYS25/CSYS25/D021S005R003/4625024/sname-csys-2025-015.pdf/1 by Martin Kjellberg on 28 May 2025

$$\mathrm{SA}(t) = f\left(\mathrm{AWA}\big(\boldsymbol{V}_{TW}(\boldsymbol{X}(t), t), \boldsymbol{V}_{\mathrm{S}}(t), \psi(t)\big)\right). \tag{6}$$

This approach ensures real-time responsiveness to changing wind conditions, only limited by the finite sheeting angular rate.

3.1.1 Reactive Intermittent Control

RIC adjusts the sheet angle intermittently and only when significant changes in a moving average of the apparent wind angle is detected. This method reduces the frequency of adjustments, potentially reducing mechanical wear on the sheeting mechanism:

$$\mathrm{SA}(t) = f\left(\overline{\mathrm{AWA}}\big(\boldsymbol{V}_{TW}(\boldsymbol{X}(t), t), \boldsymbol{V}_{\mathrm{S}}(t), \psi(t)\big)\right). \tag{7}$$

Here, the apparent wind angle defined in equation (4) is averaged over a time T_{past}:

$$\overline{\mathrm{AWA}}\big(\boldsymbol{V}_{TW}(\boldsymbol{X}(t), t), \boldsymbol{V}_{\mathrm{S}}(t), \psi(t)\big) = \frac{1}{T}\int_{t-T_{\mathrm{past}}}^{t} \mathrm{AWA}\big(\boldsymbol{V}_{TW}(\boldsymbol{X}(\tau), \tau), \boldsymbol{V}_{\mathrm{S}}(\tau), \psi(\tau)\big)\, d\tau\,. \tag{8}$$

The condition for triggering adjustment is defined as

$$\left|\overline{\mathrm{AWA}}\big(\boldsymbol{V}_{TW}(\boldsymbol{X}(t), t), \boldsymbol{V}_{\mathrm{S}}(t), \psi(t)\big) - \mathrm{AWA}_{\mathrm{ref}}\right| \geq \Delta\mathrm{AWA}_{\mathrm{threshold}}, \tag{9}$$

where $\mathrm{AWA}_{\mathrm{ref}}$ is the reference apparent wind angle updated after each adjustment and $\Delta\mathrm{AWA}_{\mathrm{threshold}}$ is the predefined threshold for triggering adjustments.

When triggered, the sheet angle is adjusted according to the current moving average and the reference apparent wind angle is reset:

$$\mathrm{AWA}_{\mathrm{ref}} \leftarrow \overline{\mathrm{AWA}}\big(\boldsymbol{V}_{TW}(\boldsymbol{X}(t), t), \boldsymbol{V}_{\mathrm{S}}(t), \psi(t)\big). \tag{10}$$

3.1.2 Predictive Intermittent Control

PIC is like RIC but incorporates foresight into the control mechanism by anticipating future apparent wind angles based on the vessel's projected trajectory, allowing for proactive adjustments to the sheet angle.

In reality, remote sensing of the ambient wind field and forecasting to the projected trajectory would also be required. However, as mentioned earlier, in this paper we rely on the fact that we can sample the deterministic spatio-temporal wind model at any point in time and space.

The vessel's projected trajectory is calculated as a linear motion extrapolation to time $t + \Delta t$:

$$\boldsymbol{X}(t + \Delta t) = \boldsymbol{X}(t) + \overline{\boldsymbol{V}_{\mathrm{S}}}(t) \cdot \Delta t, \tag{11}$$

where $\overline{\boldsymbol{V}_{\mathrm{S}}}(t)$ is the current moving average horizontal velocity vector averaged over a time T, given by:

$$\overline{\boldsymbol{V}_{\mathrm{S}}}(t) = \frac{1}{T}\int_{t-T}^{t} \boldsymbol{V}_{\mathrm{S}}\, d\tau. \tag{12}$$

Downloaded from http://onepetro.org/SNAMECSYS/proceedings-pdf/CSYS25/CSYS25/D021S005R003/4625024/sname-csys-2025-015.pdf/1 by Martin Kjellberg on 28 May 2025

The predictive moving average calculation of the apparent wind angle, including future apparent wind angles, is then calculated as:

$$\overline{\mathrm{AWA}}\left(\boldsymbol{V}_{TW}(\boldsymbol{X}(t),t),\boldsymbol{V}_{\mathrm{S}}(t),\psi(t)\right)=\frac{1}{T_{\mathrm{past}}+T_{\mathrm{future}}}\int_{t-T_{\mathrm{past}}}^{t+T_{\mathrm{future}}}\mathrm{AWA}\left(\boldsymbol{V}_{TW}(\boldsymbol{X}(\tau),\tau),\boldsymbol{V}_{\mathrm{S}}(\tau),\psi(\tau)\right)d\tau. \quad (13)$$

Finally, the sheet angles are again given by the mapping function f and the condition for triggering adjustment is again given by (9) and the reference apparent wind angle is reset according to (10).

3.2 Rudder

A proportional–integral–derivative (PID) autopilot controls the rudder and in this study a course control mode was used, ensuring that over time, a target course over ground is obtained. The ordered rudder angle is given by:

$$\delta_{\mathrm{order}}(t)=K_{\mathrm{P}}\left((\mathrm{COG}_{\mathrm{FP}}(t)-\mathrm{COG}_0)+\frac{1}{T_{\mathrm{I}}}\int_0^t e(\tau)\,d\tau+T_{\mathrm{D}}\,\dot{\psi}(t)\right), \quad (14)$$

where K_{P} is the coefficient for the proportional term. T_{I} and T_{D} represent the integration time and a derivative time respectively. $\mathrm{COG}_{\mathrm{FP}}$ is the course over ground at the fore perpendicular, COG_0 is the target course over ground and $\dot{\psi}$ is the yaw rate.

5. CASE DESCRIPTION

The test case used in this study is the wind-assisted general cargo vessel *SWOPP II*, designed in-house for the “RISE-SSPA Workshop on Performance Prediction for Wind-Powered Ships” (SWOPP Project, 2024). The vessel, designed by RISE for the workshop, features four two-element rigid wing sails, each with a projected area of 138 m^2, a controllable pitch propeller, and a hypothetical electric propulsion system with a maximum power of 700 kW.

The vessel’s total sail area of the vessel is relatively large at 552 m^2, as can be seen in Figure 3, resulting in power savings in the order of 30-40%, depending on route and speed.

The main particulars of the vessel are given in Table 1.

Downloaded from http://onepetro.org/SNAMECSYS/proceedings-pdf/CSYS25/CSYS25/D021S005R003/4625024/sname-csys-2025-015.pdf/1 by Martin Kjellberg on 28 May 2025

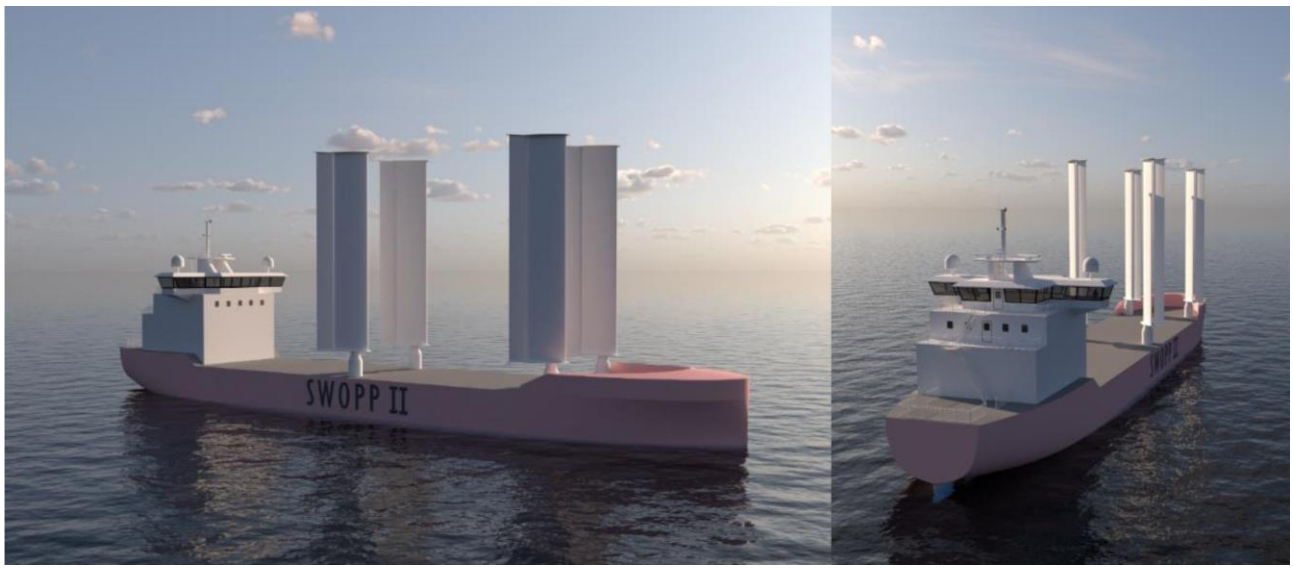

Figure 3. Rendering of the *SWOPP II* general cargo vessel with four 138 m^2 two-element rigid wing sails.

Table 1. Main particulars of the *SWOPP II* general cargo vessel.

Parameter	Value
Length between perpendiculars	88.3 m
Breadth, moulded	15.0
Design draught, moulded (fore / aft)	4.2/4.2 m
Volume displacement	4 130 m^3
Maximum Propulsive Power (MPP)	700 kW
Propeller diameter	3.0 m
Wind propulsion system	4 generic two-element wings
Wing sail span	23.0 m
Chord (main wing)	4.0 m
Chord (flap)	2.0 m

5.1 Test Parameters and Conditions

The initial conditions in terms of ship speed, sheet angles and engine power are determined by motor sailing in calm water and steady wind and adjusting the engine power until the ship speed over ground converges to 8 kn. The engine power in the rest of the simulations is then kept constant and only the autopilot and the sheet controllers are active. This means, however, that the average speed in these simulations will not be 8 kn, but typically lower due to added resistance due to waves and non-optimal sheet angles in the varying and gusty wind. An example of one of the simulations in calm water and steady wind is illustrated in Figure 4, where the TWA is 55°.

Downloaded from http://onepetro.org/SNAMECSYS/proceedings-pdf/CSYS25/CSYS25/D021S005R003/4625024/sname-csys-2025-015.pdf/1 by Martin Kjellberg on 28 May 2025

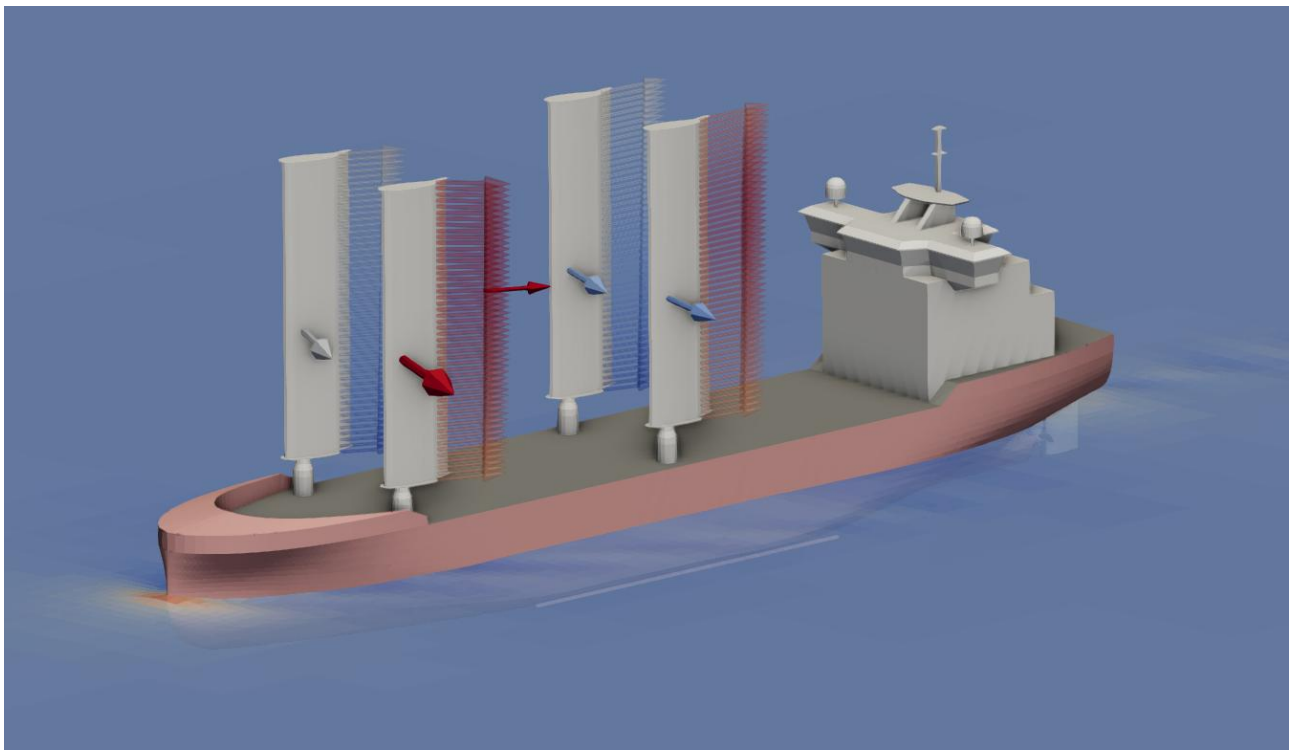

Figure 4 The vessel motor sailing in calm water and steady wind to determine required the engine power to make 8 kn speed over ground in a TWS of 7 m/s and a TWA of 55°. The four arrows on the quarter-chord line represent the individual wing sail force vectors and the arrows along the three-quarter chord line represent the local wind velocity as used by the lifting line. Finally, the single arrow in between the wing sails represent the undisturbed AWA used by the sheet controller.

The autopilot parameters were set to $K_\mathrm{P} = 2$, $T_\mathrm{I} = 30$ s and $T_\mathrm{D} = 60$ s. The sheet control parameters used with the different sheet control algorithms are given in Table 2.

Table 2. Sheet control parameters

Sheet control	T_{past} [s]	T_{future} [s]	$\Delta\mathrm{AWA}_{\mathrm{threshold}}$ [°]	$\mathrm{SA}_{\mathrm{buffer}}$ [°]	Sheet rate [° s^{-1}]
RCC	N/A	N/A	N/A	3.0	2.0
RIC	40.0	0.0	3.0	3.0	2.0
PIC	20.0	20.0	3.0	3.0	2.0

The case definitions are shown in Table 3, where the environmental conditions in terms of wind and waves are provided along with the engine power.

Table 3. Test program.

Case	TWS [m s^{-1}]	TWA [°]	H_s [m]	T_z [s]	Wave spectrum	P_D [kW]	Sheet control
RCC-55	7.0	55	0.88	5.3	JONSWAP	144	RCC
RIC-55	7.0	55	0.88	5.3	JONSWAP	144	RIC
PIC-55	7.0	55	0.88	5.3	JONSWAP	144	PIC
RCC-90	7.0	90	0.88	5.3	JONSWAP	33	RCC
RIC-90	7.0	90	0.88	5.3	JONSWAP	33	RIC
PIC-90	7.0	90	0.88	5.3	JONSWAP	33	PIC
RCC-150	7.0	150	0.88	5.3	JONSWAP	137	RCC
RIC-150	7.0	150	0.88	5.3	JONSWAP	137	RIC

Downloaded from http://onepetro.org/SNAMECSYS/proceedings-pdf/CSYS25/CSYS25/D021S005R003/4625024/sname-csys-2025-015.pdf/1 by Martin Kjellberg on 28 May 2025

PIC-150	7.0	150	0.88	5.3	JONSWAP	137	PIC

6. RESULTS

The simulation results are summarized in Table 4, which included the average speed over ground V_S, the propeller thrust $F_{x,prop}$, the total longitudinal sail force $F_{x,sails}$ and the "propulsive ratio" (PR), defined as:

$$PR = \frac{F_{x,sails}}{F_{x,prop} + F_{x,sails}} \tag{15}$$

Time series of true wind speed, total sail force, speed over ground, and apparent wind angle are plotted in Figures 5–7 for the TWA = 55°, 90° and 150° cases, respectively.

Table 4. Summary of results from the simulations.

Case	TWA [°]	Sheet control	V_S [kn]	$F_{x,prop}$ [kN]	$F_{x,sails}$ [kN]	PR [%]	Sheet adj. / min
RCC-55	55	RCC	7.51	35.1	26.1	42.6	N/A
RIC-55	55	RIC	7.41	35.3	25.4	41.9	0.87
PIC-55	55	PIC	7.47	35.2	25.9	42.4	0.90
RCC-90	90	RCC	6.94	10.0	29.2	74.5	N/A
RIC-90	90	RIC	6.16	11.2	20.8	65.0	3.10
PIC-90	90	PIC	6.74	10.3	27.3	72.6	5.47
RCC-150	150	RCC	7.97	32.8	14.9	31.3	N/A
RIC-150	150	RIC	7.84	33.0	13.3	28.7	4.17
PIC-150	150	PIC	7.94	32.8	14.6	30.8	9.13

The propulsive ratio is highest in the TWA = 90° cases, ranging from 65.0% to 74.5%, which also corresponds to the largest speed reduction from the calm water and steady wind speed of 8 kn. For TWA = 55°, the propulsive ratio is around 42%, and for TWA = 150°, it is around 30%. The smallest speed reduction is observed in the TWA = 150° cases.

The most significant performance difference between the three sheet control algorithms occurs at TWA = 90°. The RCC algorithm achieves a propulsive ratio of 74.5%, closely followed by the PIC algorithm at 72.6%. The RIC algorithm, however, results in a lower propulsive ratio of 65.0%, which is a reduction of 9.5 percentage points. For TWA = 55° and 150°, the differences in propulsive ratio are much smaller, with a maximum variation of 2.6 percentage points between the RIC and RCC algorithms.

The frequency of sheet adjustments is significantly higher for TWA = 90° and 150° where the variability of the apparent wind angle is larger, especially for TWA = 150°.

Downloaded from http://onepetro.org/SNAMECSYS/proceedings-pdf/CSYS25/CSYS25/D021S005R003/4625024/sname-csys-2025-015.pdf/1 by Martin Kjellberg on 28 May 2025

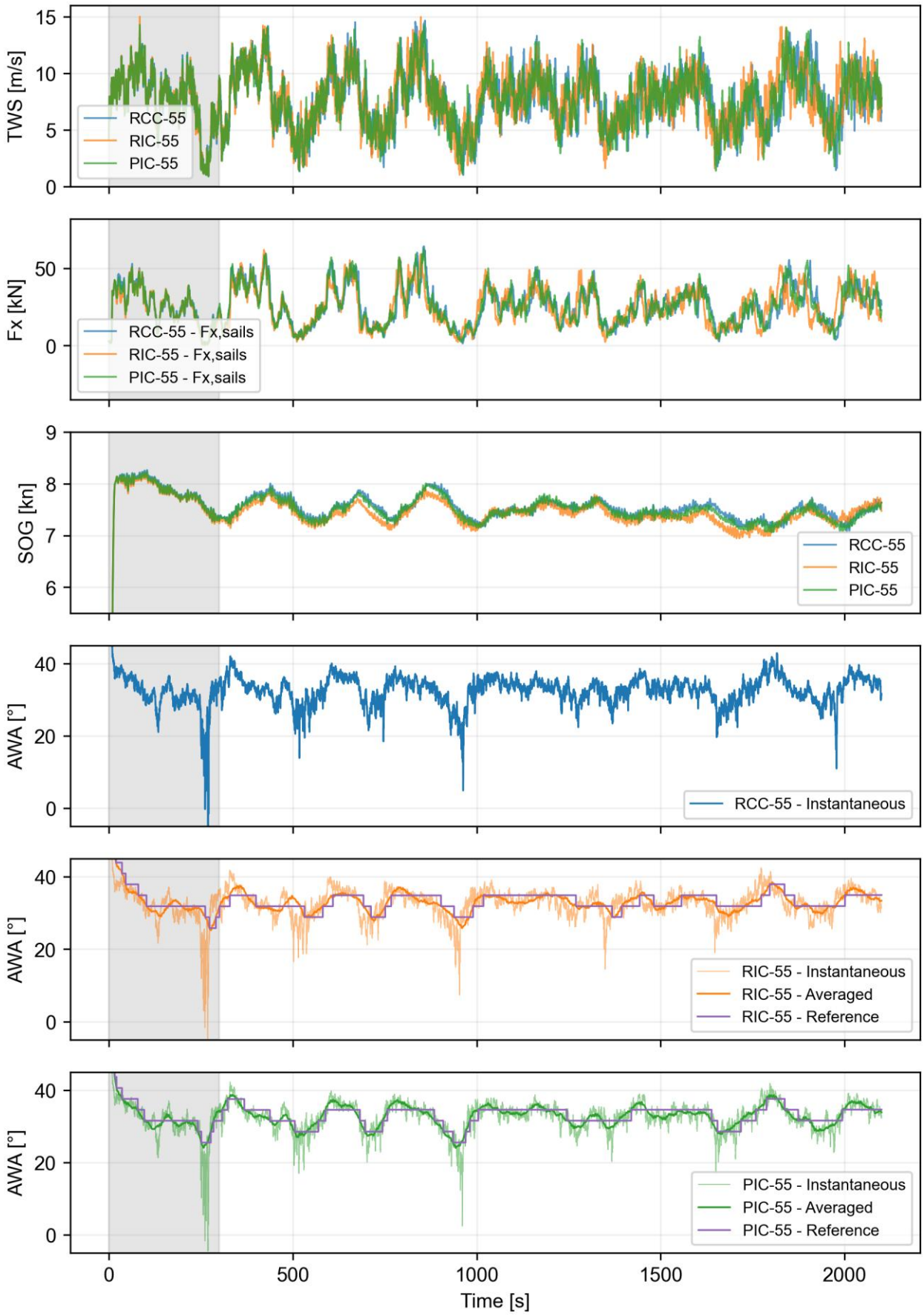

Figure 5. Time series for TWA = 55°. The first 300 s (grey) are excluded from the analysis.

Downloaded from http://onepetro.org/SNAMECSYS/proceedings-pdf/CSYS25/CSYS25/D021S005R003/4625024/sname-csys-2025-015.pdf/1 by Martin Kjellberg on 28 May 2025

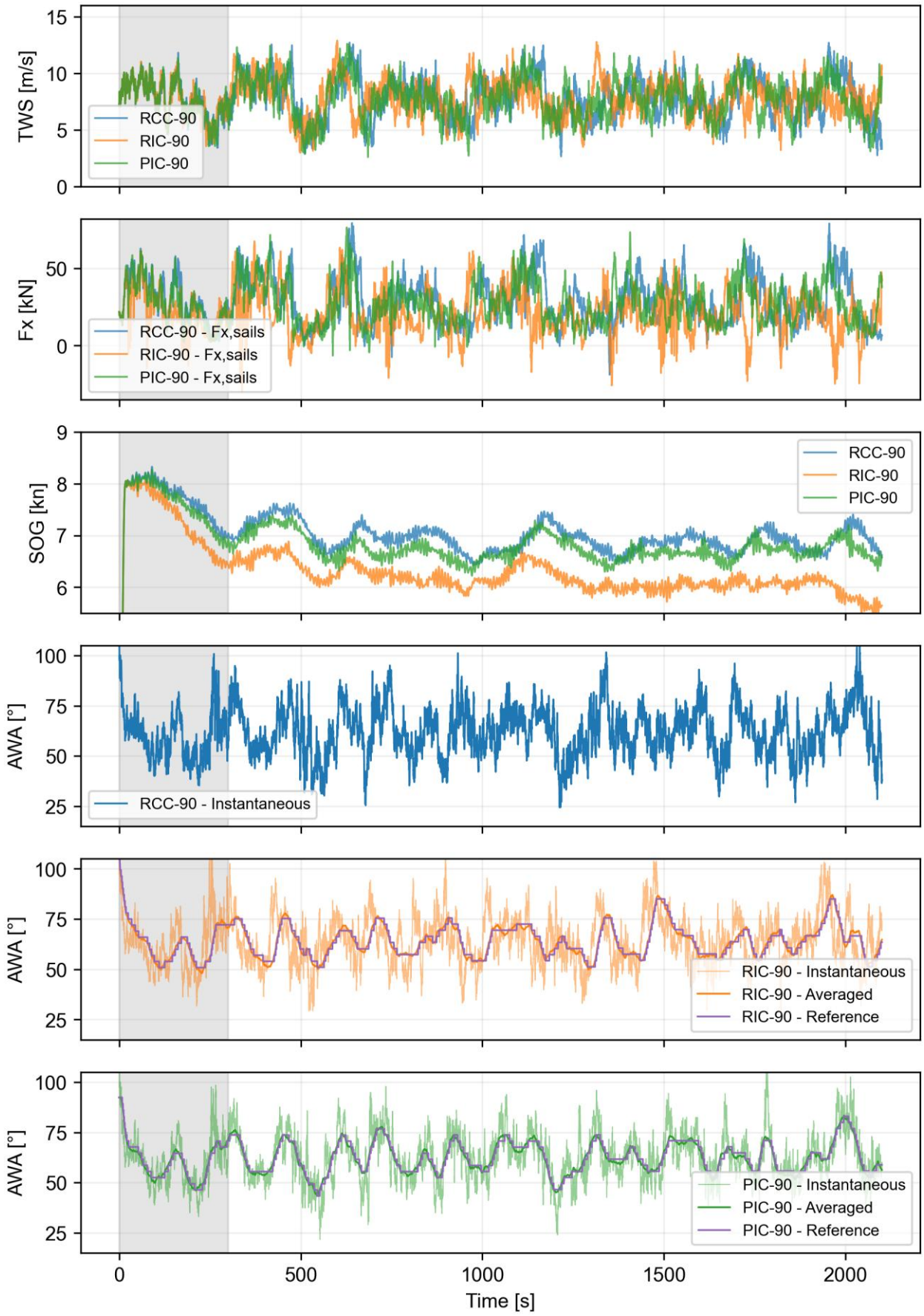

Figure 6. Time series for TWA = 90°. The first 300 s (grey) are excluded from the analysis.

Downloaded from http://onepetro.org/SNAMECSYS/proceedings-pdf/CSYS25/CSYS25/D021S005R003/4625024/sname-csys-2025-015.pdf/1 by Martin Kjellberg on 28 May 2025

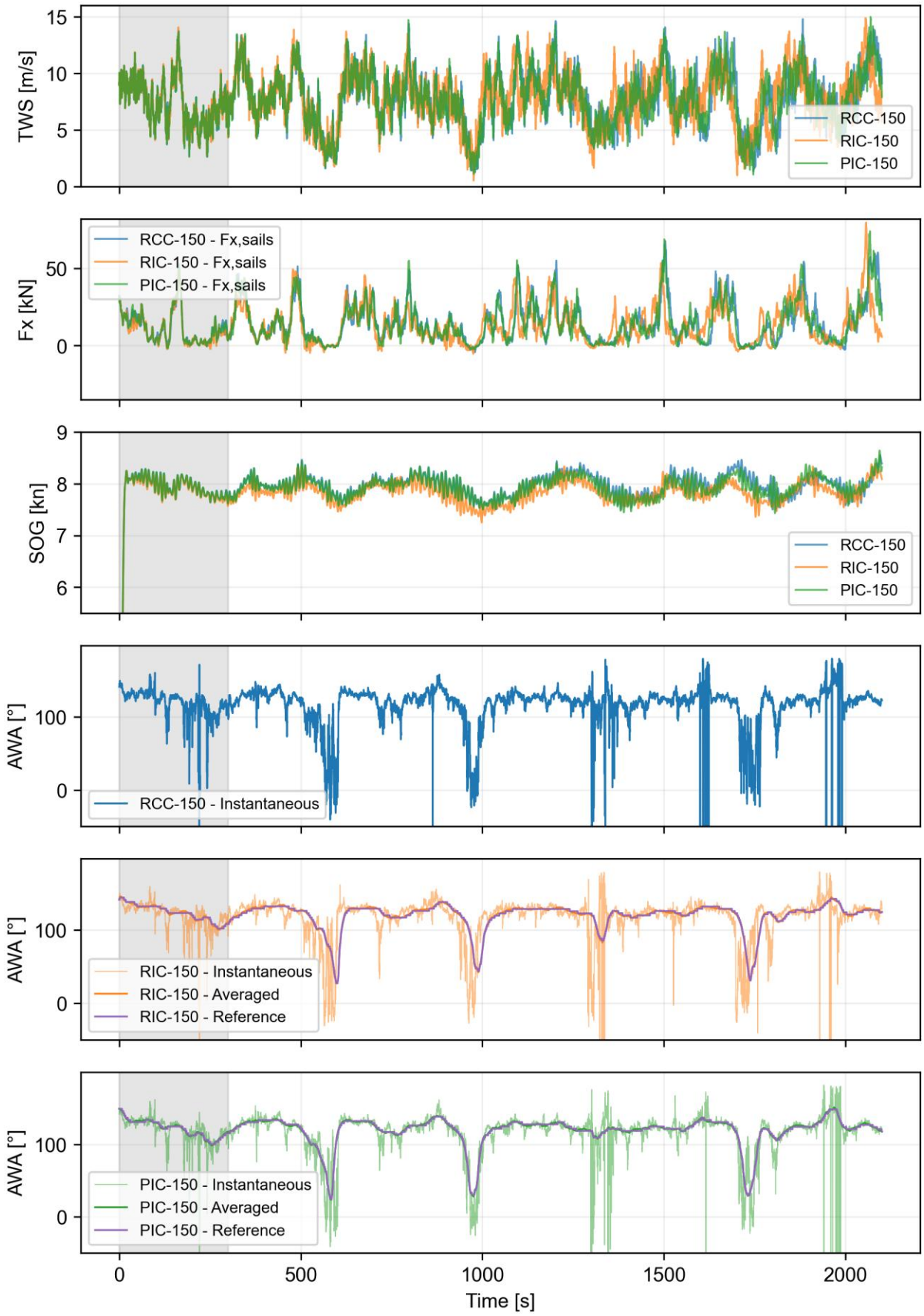

Figure 7. Time series for TWA = 150°. The first 300 s (grey) are excluded from the analysis.

Downloaded from http://onepetro.org/SNAMECSYS/proceedings-pdf/CSYS25/CSYS25/D021S005R003/4625024/sname-csys-2025-015.pdf/1 by Martin Kjellberg on 28 May 2025

7. CONCLUSIONS

This study explored the impact of three different sheet control algorithms, Reactive Continuous Control (RCC), Reactive Intermittent Control (RIC) and Predictive Intermittent Control (PIC), on the sailing performance of a wind-assisted general cargo vessel. The investigation made use of a deterministic spatio-temporal wind model, enabling a direct comparison of the performance of the three approaches in varying true wind directions.

Key conclusions drawn from the study are as follows:

Performance across different true wind angles: The effectiveness of the sheet control algorithms is highly dependent on the TWA. The highest propulsive ratios were observed at TWA = 90°, with values ranging from 65.0% to 74.5%. These conditions demonstrated the most significant performance variations between the algorithms.

For TWA = 55° and 150°, the differences in propulsive ratios among the algorithms were minimal, with variations of less than 3 percentage points, highlighting that the choice of algorithm is less critical in these conditions.

Algorithm-specific observations: Reactive Continuous Control (RCC) achieved the highest propulsive ratios in most cases, particularly at TWA = 90°, indicating superior aerodynamic performance due to its real-time responsiveness to apparent wind angle changes. However, this comes at the potential cost of higher mechanical wear and energy usage due to the continuous adjustments.

Reactive Intermittent Control (RIC) showed reduced performance, particularly at TWA = 90°, where its propulsive ratio was 9.5 percentage points lower than for the RCC. Despite this, with sheet adjustment rates ranging from 0.87 to 4.17 adjustments per minute across different true wind angles, RIC offers the advantage of potentially reduced mechanical wear and lower energy consumption, making it a practical choice for scenarios with less wind variability.

Predictive Intermittent Control (PIC) provided a balance between performance and system efficiency. It nearly matched RCC in propulsive ratio, even at TWA = 90%, and showed sheet adjustment rates between 0.90 and 9.13 adjustments per minute, noting, however, that the latter was the highest rate observed. PIC showed promise for future implementation with remote wind sensing and predictive forecasting capabilities.

Impact of apparent wind angle variability: Conditions with higher variability in the apparent wind angle, such as TWA = 150°, resulted in increased frequency of sheet adjustments. RCC's responsiveness provided consistent performance, while RIC and PIC demonstrated reduced mechanical activity, which could benefit long-term durability and impact energy consumption.

Overall system performance: The results confirm that effective sheet control strategies may significantly influence the propulsive performance of wind propulsion systems. The choice of algorithm must consider the trade-offs between performance, energy usage, and mechanical wear, depending on operational priorities and environmental conditions.

RCC offers superior performance with higher adjustment rates, RIC provides lower adjustment rates with significant performance loss in some conditions, and PIC balances both aspects with high performance and lower adjustment rates based on predictive capabilities. The costs of energy usage and mechanical wear, however, were not quantified in this study.

Downloaded from http://onepetro.org/SNAMECSYS/proceedings-pdf/CSYS25/CSYS25/D021S005R003/4625024/sname-csys-2025-015.pdf/1 by Martin Kjellberg on 28 May 2025

As a final note, this study assumes ideal performance of local on-board or remote wind measurements. Therefore, the results demonstrate the potential of the sheet control algorithms, which may be challenging to achieve fully in practical applications.

8. FUTURE WORK

Future work should focus on:

- Sensitivity of sheet controller parameters, such as averaging time constants and sheet angle buffer.
- Investigate a wider range of sailing conditions, i.e. TWS, TWA, ship speed, etc.
- Developing and testing a model of an on-board LIDAR system to simulate realistic remote sensing of the ambient wind field.
- Development of forecasting algorithms to be used together with the remote sensing system.
- Further development of more complex and capable control algorithms and strategies.
- Combined control of sails and rudder.

ACKNOWLEDGEMENTS

This work received funds from the European Union's Horizon Europe Research and Innovation programme under grant no. 101096673 – Orcelle Horizon, and the European Climate, Infrastructure and Environment Executive Agency (CINEA), Project 101056769 – OPTIWISE. The authors are especially grateful to the anonymous Reviewers for their generous help in improving the article.

REFERENCES

Anderson, John D., Stephen Corda, and David M. Van Wie (1980). "Numerical lifting line theory applied to drooped leading-edge wings below and above stall". In: *Journal of Aircraft* 17.12, pp. 898–904. ISSN: 00218669. DOI: 10.2514/3.44690.

Cole, Kenan (2018). "Reactive trajectory generation and formation control for groups of UAVs in windy environments". PhD thesis. The George Washington University.

Kjellberg, M., F.C. Gerhardt, and S. Werner (2023). "Sailing Performance of Wind-Powered Cargo Vessel in Unsteady Conditions", Journal of Sailing Technology, Volume 8, pp. 218–254. doi:10.5957/jst/2023.8.12.218.

Malmek, K. et al. (2020). "Comparison of two rapid numerical methods for predicting the performance of multiple rigid wing-sails". In: *Proceedings of 5th International Conference on Innovation in High Performance Sailing Yachts and Sail-Assisted Ship Propulsion*.

SWOPP Project (2024). *Joint Industry Project: RISE-SSPA Workshop on Performance Prediction for Wind-Powered Ships (SWOPP)*. Retrieved from https://www.ri.se/en/what-we-do/projects/joint-industry-project-performance-prediction-wind-powered-ships in November 2024.

Downloaded from http://onepetro.org/SNAMECSYS/proceedings-pdf/CSYS25/CSYS25/D021S005R003/4625024/sname-csys-2025-015.pdf/1 by Martin Kjellberg on 28 May 2025